SCIENTIFIC REPORTS

OPEN

SUBJECT AREAS:
ELECTRONIC PROPERTIES AND MATERIALS
THERMOELECTRICS

Received
10 July 2014

Accepted
4 December 2014

Published
8 January 2015

Correspondence and requests for materials should be addressed to X.-L.W. (xiaolin@uow.edu.au)

Superior intrinsic thermoelectric performance with *zT* of 1.8 in single-crystal and melt-quenched highly dense $Cu_{2-x}Se$ bulks

Lan-ling Zhao[1,2], Xiao-lin Wang[1], Ji-yang Wang[2], Zhen-xiang Cheng[1], Shi-xue Dou[1], Jun Wang[1] & Li-qiang Liu[3]

[1]Spintronic and Electronic Materials Group, Institute for Superconducting and Electronic Materials, Australian Institute for Innovative Materials, University of Wollongong, North Wollongong, 2500, Australia, [2]Institute for Crystal Materials, Shandong University, Jinan, Shandong, P.R. China, [3]Faculty of Engineering, Shandong Jianzhu University, Shandong, P.R. China.

Practical applications of the high temperature thermoelectric materials developed so far are partially obstructed by the costly and complicated fabrication process. In this work, we put forward two additional important properties for thermoelectric materials, high crystal symmetry and congruent melting. We propose that the recently discovered thermoelectric material $Cu_{2-x}Se$, with figure of merit, *zT*, over 1.5 at *T* of ~ 1000 K, should meet these requirements, based on our analysis of its crystal structure and the Cu-Se binary phase diagram. We found that its excellent thermoelectric performance is intrinsic, and less dependent on grain size, while highly dense samples can be easily fabricated by a melt-quenching approach. Our results reveal that the melt-quenched samples and single crystals exhibit almost the same superior thermoelectric performance, with *zT* as high as 1.7–1.8 at *T* of ~973 K. Our findings not only provide a cheap and fast fabrication method for highly dense $Cu_{2-x}Se$ bulks with superior thermoelectric performance, paving the way for possible commercialization of $Cu_{2-x}Se$ as an outstanding component in practical thermoelectric modules, but also provide guidance in searching for new classes of thermoelectric systems with high crystal symmetry or further improving the cost performance of other existing congruent-melting thermoelectric materials.

High temperature thermoelectric (TE) technology has been increasingly significant for a sustainable and environmental friendly supply of clean energy, due to our increasingly severe environmental problems and the energy crisis[1–3]. Thermal energy can be converted into electricity directly when a temperature gradient is formed on TE junctions[4–7]. TE devices can work with high reliability, quiet operation due to the lack of moving parts, and no pollution[8–10].

Many alloys and nanostructured materials, such as Co_4Sb_{12}, β-Zn_4Sb_3, and PbTe or PbSe-based alloys, have been investigated extensively and developed as high temperature TE materials for power generation[11–17]. Their TE performance has been improved greatly, with the thermoelectric figure-of-merit over 1. It is well known that the energy conversion efficiency of TE materials at a temperature T can be evaluated by the dimensionless thermoelectric figure-of-merit (zT) defined as $zT = S^2T/\rho\kappa$, where S, T, ρ, and κ are the Seebeck coefficient, absolute temperature, electrical resistivity, and total thermal conductivity, respectively[18–23]. κ can be expressed by $\kappa = \kappa_L + \kappa_c$, where κ_L and κ_c are the lattice thermal conductivity and the charge carrier thermal conductivity, respectively. Lattice or atomic vibrations contribute predominantly to κ at high temperatures compared to those of the charge carriers.

Among these parameters, κ is the decisive factor ruling the TE performance, as it determines the heat transport capability between the hot and cold sides of the TE modules. Therefore, reducing κ has been the main focus of studies aiming to improve zT for various types of high temperature TE materials in particular. The following effective approaches have been commonly used so far to reduce κ through phonon refinement: 1) reducing particle sizes to the nanoscale using nano-engineering, which gives rise to both intragrain and intergrain (grain boundary) phonon confinement; 2) fabricating multilayer thin films to reduce the dimensionality of TE materials; and 3) doping with heavy atoms to effectively reduce the phonon vibrations.

Nevertheless, the fabrication methods employed for multilayer thin films and nanoparticles involve costly equipment that is capable of operating under conditions of high vacuum, high temperature, and high pressure, as well as complicated chemical processes. Highly dense polycrystalline TE bulks are commonly synthesized by the hot pressing method under high temperature and high pressure, using expensive spark plasma sintering (SPS) systems. They are all very costly and long heat treatments are needed (usually up to several days), making TE materials less suitable for practical applications. Therefore, it is much more attractive to find an effective fabrication method that is low-cost and time-saving.

In this work, we propose to achieve highly dense samples with excellent TE performance for a certain type of thermoelectric compound by employing a low-cost and time-saving method based on the following facts and analyses: 1). Materials possessing the congruent melting property should maintain the same chemical phase and composition from the homogeneous melt state to the solid state, despite subtle differences in the real chemical compositions of the solid and melt states due to possible loss of volatile element(s) above the melting temperature. This means that highly dense bulks should be easily obtained by the melt-quenching approach. This has been successfully adopted in single crystal growth and casting technology for various materials, giving highly density and excellent performance, although little work has been done on the fabrication of polycrystalline TE materials[24–27]. 2). Anisotropy plays a significant role in the TE performance of a material with anisotropic crystal structure or low crystal symmetry[28,29]. It should be noted that the anisotropy is an important or an additional factor that is likely to affect the overall TE performance of polycrystalline bulk samples, and it needs to be taken into account in the consideration of zT improvement.

Materials showing excellent TE performance, such as Bi_2Te_3, exhibit high anisotropy in their crystal structures, which is likely to be the reason why polycrystalline bulks have lower zT than the corresponding single crystals with certain preferred crystallographic directions. Inspired by the above considerations, for cubic-structured TE materials, their TE performances along the three main crystallographic axes (a, b, and c directions) should be the same due to the identical arrangement of atoms along these equivalent directions. Grain boundaries or particle sizes should have less effect on κ and other TE parameters in cubic-structured TE materials compared to those with low crystal symmetry. Therefore, we propose two additional properties for excellent TE materials: congruent melting and high crystal symmetry, or at least less anisotropy.

It has come to our attention that the recently discovered new class of copper ion liquid-like TE material, $Cu_{2-x}Se$, ought to meet these requirements. $Cu_{2-x}Se$ bulks prepared by the hot pressing method show high TE performance with $zT > 1.5$ at T of $\sim$ 1000 K[30,31]. Its high temperature β-phase has the cubic crystal structure with space group $Fm\bar{3}m$, and the copper ions can behave like a liquid, which could lead to similar TE performance between single crystals and polycrystalline bulks at high temperatures.

Figure 1 shows the binary phase diagram of the Cu-Se system[32–34] and the assumed ideal unit cell of the high temperature β-phase $Cu_{2-x}Se$[35]. According to this binary phase diagram, the low temperature α-phase $Cu_{2-x}Se$ is transformed to the high-temperature β-phase at $\sim$ 400 K and seems to undergo a congruent melting at

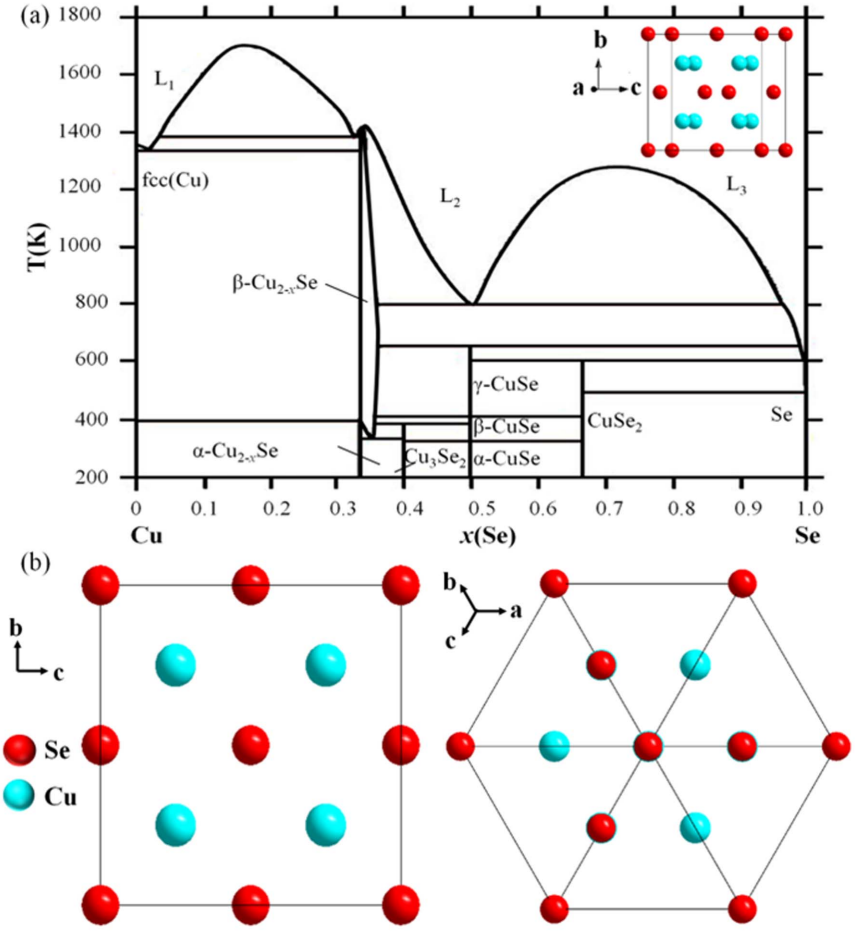

Figure 1 | (a) Binary phase diagram of the Cu-Se system. The inset shows the 3D unit cell of high temperature β-phase $Cu_{2-x}Se$. (b) Unit cell of high temperature β-phase $Cu_{2-x}Se$ viewed towards the (100) and (111) planes, respectively.

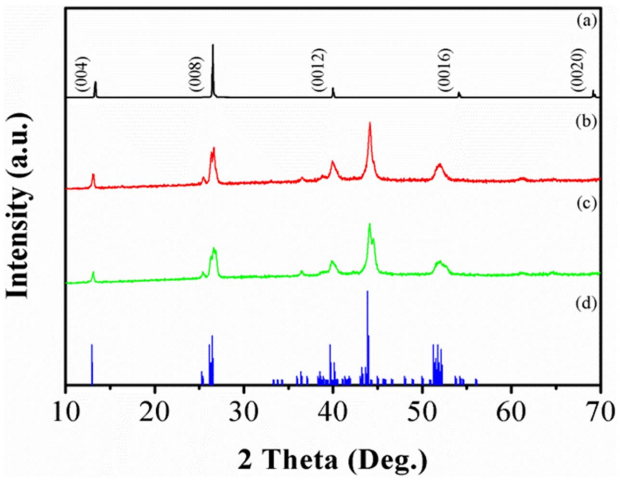

Figure 2 | X-ray diffraction patterns for as-prepared samples: (a) $Cu_{2-x}Se$ single crystals grown by a modified Bridgman method. (b) water-quenched $Cu_{2-x}Se$ bulks. (c) LN-quenched $Cu_{2-x}Se$ bulks. (d) standard XRD peaks of low temperature α-phase $Cu_{2-x}Se$ (PDF No. 27-1131).

~ 1400 K. Therefore, we can expect that highly dense $Cu_{2-x}Se$ bulks could be obtained by a melting and quenching (or melt-quenching) method. As this compound can be copper deficient, we must discuss the melting process for this compound.

Congruent melting occurs during melting of a compound when the composition of the liquid that is formed is the same as the composition of the solid. Materials possessing the congruent melting property should maintain the same chemical phase and composition from the homogeneous melt state to the solid state, which means that highly dense bulks should be easily obtained by a melt-quenching approach.

Congruent melting is not appropriate for non-stoichiometric compounds such as $Cu_{2-x}Se$[32–34] ($x < 0.25$) and $La_{3-x}Te_4$[24] ($x < 1/3$). The exact congruent melting composition for $Cu_{2-x}Se$, has been reported to be $Cu_{1.9975}Se$[36], or $Cu_{1.9956}Se$[37], or $Cu_{1.994}Se$[38]. For $Cu_{2-x}Se$ with other x values, the melting should not be congruent, and the chemical compositions of melt-quenched samples should be different from the nominal compositions of the starting materials. This is due to the segregation of secondary phase, such as with copper precipitation. It should be pointed out, however, that the amount of the segregated phase is very tiny and often hardly seen in the X-ray diffraction (XRD) patterns for melt-quenched $Cu_{2-x}Se$ samples[30,39].

Technically speaking, the Cu_2Se and $Cu_{1.98}Se$ used for our study are not congruent melting compounds. Despite this, the tiny amount of secondary phase is not seen in our XRD patterns for our own samples. Therefore, highly dense bulks should be easily obtained by a melt-quenching approach with tiny changes in compositions compared to the starting materials.

As mentioned above, the TE performance of cubic structured materials along the three main crystallographic axises should be the same due to the identical arrangement of atoms along these equivalent directions. Specifically, the high temperature β-phase $Cu_{2-x}Se$, it has a cubic structure with space group $Fm\bar{3}m$ and a quite small bandgap[30,40]. Furthermore, the copper ions can behave as a liquid in the face-centered cubic (fcc) rigid sublattice constituted by the Se atoms. Therefore, grain boundaries or particle sizes should have less effect on this system's thermal conductivity and other TE parameters compared to systems with low crystal symmetry. Additionally, the liquid-like behavior of the copper ions is favorable for both low electrical resistivity and low thermal conductivity. Therefore, the excellent TE performance should be intrinsic and less anisotropic for the high temperature β-phase $Cu_{2-x}Se$, because it is dominated by the liquid-like copper ions.

We anticipate that as long as the $Cu_{2-x}Se$ samples have 100% density, they should show high TE performance, regardless of grain size. Based on our analysis of the binary phase diagram of the Cu-Se system, the long sintering reported for highly dense $Cu_{2-x}Se$ bulks seems to be unnecessary. The melt-quenching approach should only take a few minutes to achieve highly dense $Cu_{2-x}Se$ bulks, in contrast to the conventional hot-pressing method, which requires hours of heat treatment under high pressure and high temperature. Furthermore, there is a lack of information on what the intrinsic TE performance or zT should be for the $Cu_{2-x}Se$. Therefore, it is important to carry out experiments using $Cu_{2-x}Se$ single crystals to investigate their intrinsic TE properties, as well as for comparison purposes.

Results and Discussion

Figure 2 presents the XRD patterns of powdered $Cu_{2-x}Se$ bulks fabricated by the melt-quenching approach (quenched in water and liquid nitrogen (LN)), and of a single-crystal sample prepared by a modified Bridgman method, together with the standard X-ray diffraction (XRD) peaks of low temperature α-phase $Cu_{2-x}Se$ (PDF No. 27-1131). Its XRD pattern indicates that the single-crystal sample only shows (00l) peaks of low temperature α-phase $Cu_{2-x}Se$, demonstrating that the single crystal sample's orientation is [00l] at low temperatures. At high temperature, the low temperature α-phase is converted to β-phase. Simultaneously, the (00l) plane becomes the (111) plane, which has been previously reported for $Cu_2Se_{1-x}I_x$ bulk samples[41]. Therefore, in this work, the TE performance of our single-crystal $Cu_{2-x}Se$ sample was characterized along the (111) plane of high temperature β-phase.

We also carried out Rietveld refinements for the powdered single-crystal and polycrystalline bulk samples. The unit cell of monoclinic-structured low temperature α-phase Cu_2Se is shown in Figure S1 in the Supporting Information (SI). The refined XRD patterns and the values of the Rietveld refinement parameters (lattice parameters, R-factors, and goodness of fit (GOF)) are displayed in Figure S2 and Table S1 (SI), respectively. The results indicate that all samples have the monoclinic structure (space group $C2/c$) with some differences in the lattice parameters. No visible traces of any secondary phase were detected within the XRD resolution, which is consistent with previous reports[39–43].

Field emission scanning electron microscope (FE-SEM) images of the single-crystal, water-quenched, and LN-quenched polycrystalline $Cu_{2-x}Se$ bulks are shown in Figure 3. The single-crystal surface is extremely smooth, and its edge clearly shows the layered structure. All the melt-quenched samples are highly dense without any visible voids or porosity. The average grain size is ~ 10 μm for the water-quenched sample shown in Figure 3(c), which is slightly larger than that of the $Cu_{2-x}Se$ bulks prepared by the conventional hot-pressing method[31,42]. The LN-quenched samples also have microscale grains, although they are smaller than those in the water-quenched one. Only in the part near the surface, are there some nanoscale grains. This suggests that $Cu_{2-x}Se$ can be crystallized quickly and that it is very hard to achieve small grains for thick or large-size samples.

In order to gain insight into the real chemical compositions of our samples, we carried out the chemical analysis using energy dispersive X-ray spectroscopy (EDS), and the results for individual points and EDS mapping are displayed in Figures S3 and S4 (SI), respectively. According to the point EDS analysis, subtle variations in the real chemical composition are detected for different samples. The chemical composition is estimated to be $Cu_{2.01}Se$ for the single crystals, $Cu_{1.96}Se$ for the water-quenched sample, and $Cu_{1.94}Se$ for the LN-quenched one, respectively, which is in good agreement with our XRD refinement results. The EDS mapping for all samples indicate that both Cu and Se are distributed homogeneously inside all the samples. No Cu or Se rich regions are observed, which means that there is no Se or Cu segregation.

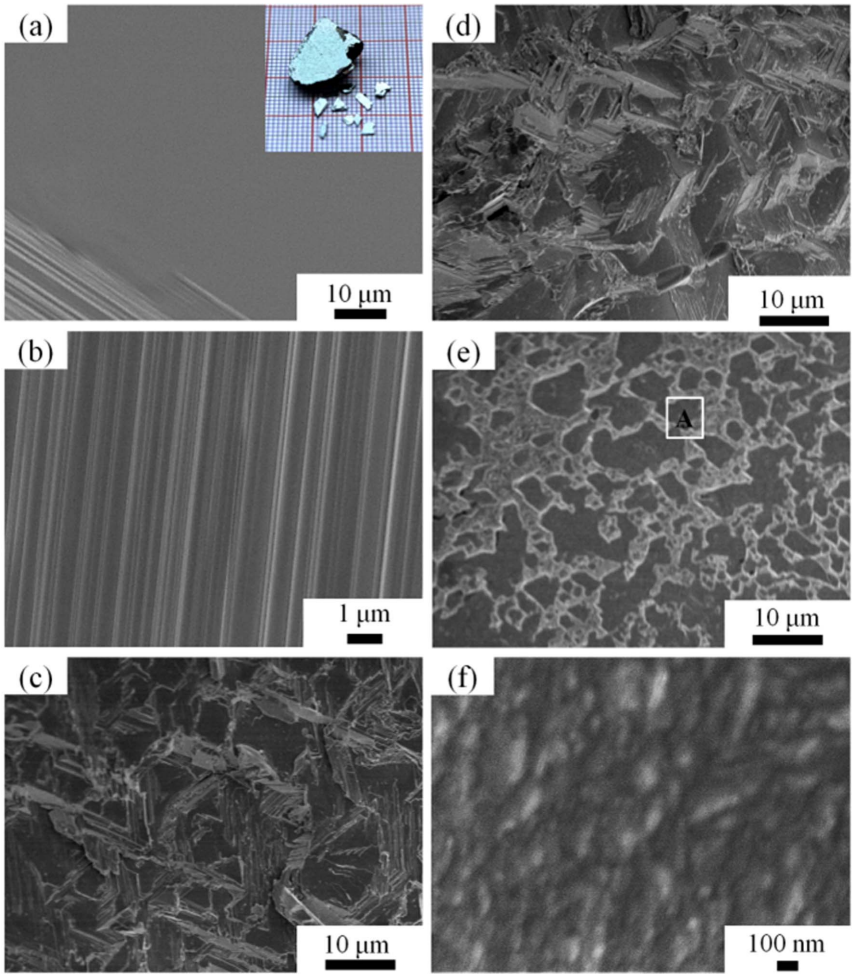

Figure 3 | **FE-SEM images of the as-prepared samples:** (a, b) Surface and cross-sectional images of single crystals. The inset shows an optical image of the $Cu_{2-x}Se$ single crystals. Cross-sectional images of water-quenched $Cu_{2-x}Se$ bulk. (c). Images of the inside (d) and near surface (e) of LN-quenched $Cu_{2-x}Se$ bulk. (f) Magnified image of region A in (e).

The temperature dependence of the electrical resistivity (ρ), Seebeck coefficient (S), total thermal conductivity (κ), power factor (PF), lattice thermal conductivity (κ_L), and thermoelectric figure-of-merit (zT) for the single-crystal, water-quenched, and LN-quenched $Cu_{2-x}Se$ samples is plotted in Figure 4. The following facts are observed: 1) The values of ρ and zT for all samples show the same trend of increasing with increasing temperature. 2) S shows almost the same value for all samples over the whole temperature range from 300 to 973 K and increases as the temperature increases. 3) κ decreases as the temperature increases for all samples. 4) The power factor, defined as $PF = S^2/\rho$, is 4-7 $\times$ 10^{-4} $W \cdot mK^{-2}$ for the low temperature α-phase and 4-11.5 $\times$ 10^{-4} $W \cdot mK^{-2}$ for the high temperature β-phase, which is comparable to the previously reported values for *conventional hot-pressed* $Cu_{2-x}Se$ samples[31].) Our LN-quenched $Cu_{2-x}Se$ sample has $zT \approx 1.5$ at T $\approx$ 973 K, which is as good as what has been reported for hot-pressed samples[30,31]. Furthermore, the zT for the water-quenched and single-crystal samples exhibits still higher values around 1.7–1.8 at $\sim$ 973 K.

It is interesting to note that compared to the water-quenched $Cu_{2-x}Se$, the LN-quenched $Cu_{2-x}Se$ with smaller grain sizes has larger ρ values ($\sim 7 \times 10^{-4}$ Ωm) and lower κ values($\sim$ 0.48 $Wm^{-1}K^{-1}$ at $\sim$ 973 K). This seems to be related to the higher density of grain boundaries which could scatter charge carriers. The Seebeck coefficient, however, is almost the same for all samples. Furthermore, the single crystal sample shows an intermediate ρ and κ among all the samples. All these data indicates that grain size may not play an important role in the TE performance of the $Cu_{2-x}Se$ system at high temperatures. This is largely due to the liquid-like behavior of the copper ions, which dominates the system's TE performance at high temperatures. Furthermore, the differences in electrical resistivity and thermal conductivity may also be related to the differences in chemical composition among the samples.

According to the Wiedemann-Franz relationship, the charge carrier thermal conductivity (κ_c) can be estimated by $\kappa_c = LT/\rho$, where L is the Lorenz number[43–45]. In this work, we take $L = 1.5 \times 10^{-8}$ $V^2 \cdot K^{-2}$ to calculate κ_c, and then subtract it from κ *to obtain* κ_L. The temperature dependence of the lattice thermal conductivity for all samples is displayed in Figure 4(e). It is interesting to note that the LN-quenched sample does not show the lowest lattice thermal conductivity, even though it has the highest density of grain boundaries compared to the other samples. For conventional TE materials, a high density of grain boundaries can effectively reduce the lattice thermal conductivity, although it seems that this is not applicable to the $Cu_{2-x}Se$ system because its high temperature β-phase is crystallized in a cubic structure with a rigid fcc sublattice constituted by the Se atoms and kinetically disordered copper ions. It is the liquid-like behavior of the copper ions that dominates the system's high temperature TE performance. The lattice thermal conductivity of both the LN-quenched and the single-crystal $Cu_{2-x}Se$ samples first decreases and then increases gently. Interestingly, we note that this phenomenon was also reported by Yu et al.[31] This could be attributed to the liquid-like behavior of the copper ions, which can confine the

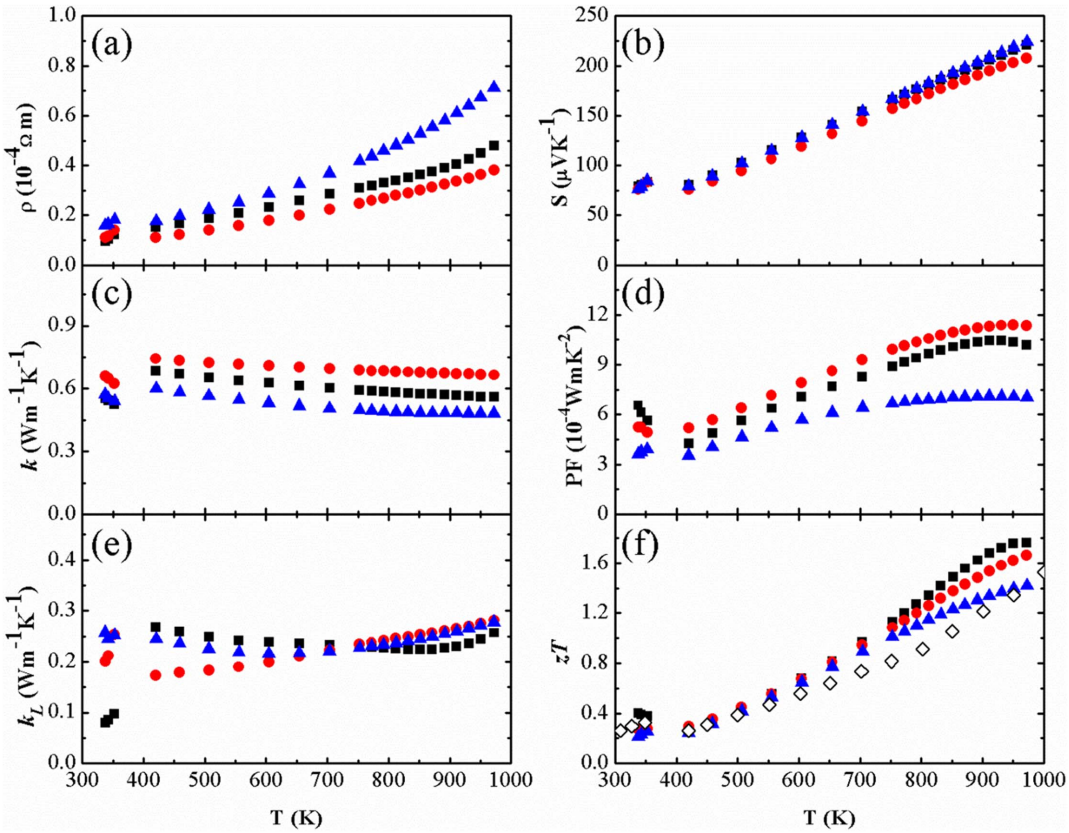

Figure 4 | Temperature dependence of thermoelectric transport properties of single-crystal and ultrfast-formed $Cu_{2-x}Se$ bulks: (a) electrical resistivity (ρ), (b) Seebeck coefficient (S), (c) total thermal conductivity (κ), (d) lattice thermal conductivity (κ_L), (e) power factor (PF), and (f) thermoelectric figure-of-merit (zT). (■ single crystals, ● water-quenched bulks, ▲ LN-quenched bulks, and ◇ polycrystalline bulks synthesized by the hot-pressing method.)

lattice vibrations and in turn reduce the lattice thermal conductivity. When the temperature is over the critical temperature (around 773 K), the lattice vibrations are mainly confined by the liquid-like copper ions, and therefore, the lattice thermal conductivity values are almost the same for all samples. As for the temperatures below the 773 K, the crystal sublattices of both the Se and the Cu atoms contribute to the lattice thermal conductivity. Additionally, subtle differences in chemical composition can also lead to different lattice thermal conductivity.

We have conducted measurements on several pieces of samples fabricated by the same method and also them repeated several times for each sample, demonstrating that our data is reproducible. The repeatability of the thermal diffusivity, electrical resistivity, and Seebeck coefficient for water-quenched $Cu_{2-x}Se$ bulks is shown in Figure S5 (SI). Our results indicate that the fast melt-quenching method works well for the fabrication of highly dense $Cu_{2-x}Se$ bulks with excellent TE performance, $zT \approx 1.7$ at 973 K, and this method should be applicable to other types of congruent-melting TE materials. It is remarkable that the fabrication cost can be reduced significantly, as the melt-quenching only takes a few minutes. We have also proposed that it is the cubic crystal symmetry and liquid-like behavior of the copper ions that makes $Cu_{2-x}Se$ show superior TE performance. Our findings pave the way for commercialization of $Cu_{2-x}Se$ as an excellent component in TE modules and can also provide guidance in searching for new classes of isotropic TE systems or further improving the cost performance of other congruent-melting TE materials. These investigations are currently underway in our group.

Methods

Sample preparation. Firstly, polycrystalline $Cu_{2-x}Se$ pellets were synthesized by a conventional solid-state method. A mixture of Cu and Se powders in the molar ratio 2-x:1 ($x = 0.02$) was pressed into pellets and sealed in evacuated quartz tubes, before being heated to 600°C for 1–5 hours with a heating rate of 5°C/min, followed by a furnace cooling to room temperature. Secondly, the as-sintered $Cu_{2-x}Se$ pellets were used in the melt-quenching approach. In order to achieve fast melting and quenching, the as-sintered samples were placed at one end of the sealed quartz tube and heated up using a flame of acetylene and oxygen until they melted completely. They were then quickly quenched in water or liquid nitrogen to obtain highly dense bulks with different grain sizes. For comparison, single crystals were also prepared using a modified Bridgman method. The as-prepared pellets were sealed in a quartz tube and melted at a temperature above 1150°C for 2 hours to obtain a homogeneous melt, followed by cooling down to 800–900°C at a rate of 1–5°C/h. The samples were then cooled to room temperature at 4°C/min.

Finally, the obtained samples were shaped into disks with dimensions of Φ10 mm × 1 mm for thermal diffusivity measurements. After the measurements, the same pieces of samples were cut into rectangular bars for measurements of the electrical resistivity and Seebeck coefficient.

Measurements. XRD patterns were collected on a GBC MMA system, and the Rietveld refinements were conducted using the Rietica software package. FE-SEM images and energy dispersive X-ray spectroscopy (EDS) for individual points and mapping was conducted with a JEOL JSM-7500FA system. The electrical resistivity and Seebeck coefficient were measured simultaneously in helium atmosphere in the temperature range from 300 to 973 K using a RZ2001i system. The thermal diffusivity (D) was measured by the laser flash method (LINSEIS LFA 1000), and the specific heat (C_p) was determined by differential scanning calorimetry (TA Q100). The sample density (dd) was determined by the Archimedes method. The thermal conductivity (κ) was calculated by $\kappa = D \times Cp \times dd$.

1. Disalvo, F. J. Thermoelectric Cooling and Power Generation. *Science* **285**, 703–706 (1999).
2. Bell, L. E. Cooling, heating, generating power, and recovering waste heat with thermoelectric systems. *Science* **321**, 1457–1461 (2008).
3. Hochbaum, A. I. *et al.* Enhanced thermoelectric performance of rough silicon nanowires. *Nature* **451**, 163–167 (2008).
4. Yang, J., Yip, H.-L. & Jen, A. K. Y. Rational Design of Advanced Theroelectric Materials. *Adv. Energy Mater.* **3**, 549–565 (2013).

5. Snyder, G. J. & Toberer, E. S. Complex thermoelectric materials. *Nature Mater.* **7**, 105–114 (2008).
6. Sales, B. C. Thermoelectric materials. Smaller is cooler. *Science* **295**, 1248–1249 (2002).
7. Rowe, D. M. (ed.) *CRC Handbook of Thermoelectrics* (*CRC,* Boca Raton, 1995).
8. Rowe, D. M. (ed.) *CRC Handbook of Thermoelectrics: Macro to Nano* (CRC, Boca Raton, 2005).
9. Nolas, G. S., Poon, J. & Kanatzidis, M. Recent developments in bulk thermoelectric materials. *MRS Bull.* **31**, 199–205 (2006).
10. Pei, Y. *et al.* Stabilizing the optimal carrier concentration for high thermoelectric efficiency. *Adv. Mater.* **23**, 5674–5678 (2011).
11. Shi, X. *et al.* Multiple-filled skutterudites: high thermoelectric figure of merit through separately optimizing electrical and thermal transports. *J. Am. Chem. Soc.* **133**, 7837–7846 (2011).
12. Toberer, E. S., Rauwel, P., Gariel, S., Taftø, J. & Jeffrey Snyder, G. Composition and the thermoelectric performance of β-Zn_4Sb_3. *J. Mater.Chem.* **20**, 9877–9885 (2010).
13. LaLonde, A. D., Pei, Y. & Snyder, G. J. Reevaluation of $PbTe_{1-x}I_x$ as high performance n-type thermoelectric material. *Energ. Environ. Sci.* **4**, 2090–2096 (2011).
14. Wang, H., Pei, Y., LaLonde, A. D. & Snyder, G. J. Weak electron-phonon coupling contributing to high thermoelectric performance in n-type PbSe. *PNAS* **109**, 9705–9709 (2012).
15. Wang, H., Pei, Y., LaLonde, A. D. & Snyder, G. J. Heavily doped p-type PbSe with high thermoelectric performance: An alternative for PbTe. *Adv. Mater.* **23**, 1366–1370 (2011).
16. Pei, Y. Z., Gibbs, Z. M., Balke, B., Zeier, W. G. & Snyder, G. J. Optimum Carrier Concentration in n-Type PbTe Thermoelectrics. *Adv. Energy Mater.* **4**, 1400486 (2014).
17. Heremans, J. P. *et al.* Enhancement of thermoelectric efficiency in PbTe by distortion of the electronic density of states. *Science* **321**, 554–557 (2008).
18. Vineis, C. J., Shakouri, A., Majumdar, A. & Kanatzidis, M. G. Nanostructured thermoelectrics: big efficiency gains from small features. *Adv. Mater.* **22**, 3970–3980 (2010).
19. Zebarjadi, M., Esfarjani, K., Dresselhaus, M. S., Ren, Z. F. & Chen, G. Perspectives on thermoelectrics: From fundamentals to device applications. *Energ. Environ. Sci.* **5**, 5147–5162 (2012).
20. Liu, W., Yan, X., Chen, G. & Ren, Z. Recent advances in thermoelectric nanocomposites. *Nano Energy* **1**, 42–56 (2012).
21. Chen, G., Dresselhaus, M. S., Dresselhaus, G., Fleurial, J. P. & Caillat, T. Recent developments in thermoelectric materials. *Int. Mater. Rev.* **48**, 45–66 (2003).
22. Jood, P. *et al.* Al-doped zinc oxide nanocomposites with enhanced thermoelectric properties. *Nano Lett.* **11**, 4337–4342 (2011).
23. Zhang, Y., Wang, X. L., Yeoh, W. K., Zheng, R. K. & Zhang, C. Electrical and thermoelectric properties of single-wall carbon nanotube doped Bi_2Te_3. *Appl. Phys. Lett.* **101**, 031909 (2012).
24. May, A., Fleurial, J.-P. & Snyder, G. Thermoelectric performance of lanthanum telluride produced via mechanical alloying. *Phys. Rev. B* **78**,125205 (2008).
25. Snyder, G. J., Christensen, M., Nishibori, E., Caillat, T. & Iversen, B. B. Disordered zinc in Zn_4Sb_3 with phonon-glass and electron-crystal thermoelectric properties. *Nature Mater.* **3**, 458–463 (2004).
26. Yu, H. *et al.* CW and Q-switched laser output of LD-end-pumped 1.06 μm c-cut Nd:$LuV0_4$ laser. *Opt. Express* **15**, 3206–3211 (2007).
27. Wu, K. *et al.* Thermal and laser properties of Nd:$Lu_3Sc_{1.5}Ga_{3.5}O_{12}$ for high power dual-wavelength laser. *Opt. Express* **20**, 6944–6951 (2012).
28. Yan, X. *et al.* Experimental Studies on Anisotropic Thermoelectric Properties and Structures of n-Type $Bi_2Te_{2.7}Se_{0.3}$. *Nano Lett.* **10**, 3373–3378 (2010).
29. Gerovac, N., Snyder, G. J. & Caillat, T. Thermoelectric Properties of n-type Polycrystalline Bi_xSb_{2-x}Te3 Alloys. *Proceedings of 2l^st^ lnternational Conference on Thermoelectronics*, Long Beach. Aug. 25–29, 2002,DOI: 10.1109/ICT.2002.1190259 (2002).
30. Liu, H. *et al.* Copper ion liquid-like thermoelectrics. *Nature Mater.* **11**, 422–425 (2012).
31. Yu, B. *et al.* Thermoelectric properties of copper selenide with ordered selenium layer and disordered copper layer. *Nano Energy* **1**, 472–478 (2012).
32. D, J. Chakrabari, D, E. L. The Cu-Se (Copper-Selenium) system. *Bull. Alloy. Phase Diagr.* **2**, 205–215 (1981).
33. Heyding, R. D. The copper selenium system. *Can. J. Chem.* **44**, 1233–1236 (1966).
34. Glazov, V. M., Pashinkin, A. S. & Fedorov, V. A. Phase equilibria in the Cu-Se system. *Inorg. Mater.* **36**, 641–652 (2000).
35. Gulay, L., Daszkiewicz, M., Strok, O. & Pietraszko, A. Crystal structure of Cu_2Se. *Chem. Met. Alloys* **4**, 200–205 (2011).
36. Lorenz, G. & Wagner, C. Investigations on Cuprous Selenide and Copper Tellurides. *J. Chem. Phys.* **26**, 1607–1608 (1957).
37. Konev, V. N., Kudinova, V. A. & Neverov, V. I. Deviations from Stoichiometry and Effective Mass of Holes in Cu_2S (S + Se) Solid Solutions. *lzv. Akad. Nauk SSSR, Neorg. Mater.* **11**, 1318–1319 (1975).
38. Glazov, V. M., Pavlova, L. M. & Asryan, A. A. Thermal Dissociation of Copper Chalcogenides during Melting. *Zh. Fiz Khim.* **70**, 5 (1996).
39. Xiao, X.-X., Xie, W.-J., Tang, X.-F. & Zhang, Q.-J. Phase transition and high temperature thermoelectric properties of copper selenide $Cu_{2-x}Se$ ($0 \leq x \leq 0.25$). *Chinese Phys. B* **20**, 087201 (2011).
40. Chrissafis, K., Paraskevopoulos, K. M. & Manolikas, C. Studying $Cu_{2-x}Se$ phase transformation through DSC examination. *J. Therm. Anal. Calorim.* **84**, 195–199 (2006).
41. Liu, H. *et al.* Ultrahigh thermoelectric performance by electron and phonon critical scattering in Cu_2Se_{1-x} I_x. *Adv. Mater.* **25**, 6607–6612 (2013).
42. Liu, H. *et al.* Structure-transformation-induced abnormal thermoelectric properties in semiconductor copper selenide. *Mater. Lett.* **93**, 121–124 (2013).
43. Mehta, R. J. *et al.* A new class of doped nanobulk high-figure-of-merit thermoelectrics by scalable bottom-up assembly. *Nature Mater.* **11**, 233–240 (2012).
44. Androulakis, J. *et al.* Spinodal decomposition and nucleation and growth as a means to bulk nanostructured thermoelectrics: enhanced performance in $Pb_{1-x}Sn_x$Te-PbS. *J. Am. Chem. Soci.* **129**, 9780–9788 (2007).
45. Bejan, A. & Kraus, A. D. (ed.) *Heat Transfer Handbook*, 1337–1338 (Wiley, New York, 2003).

Acknowledgments

L.L.Z. is grateful to the China Scholarship Council (CSC) for scholarship support. X.L.W. acknowledges support from the Australian Research Council (ARC) through an ARC Discovery Project (DP130102956) and an ARC Professorial Future Fellowship project (FT130100778). The authors would like to also thank Dr Tania Silver for critical reading of the manuscript, and also acknowledge the use of the facilities in the UOW Electron Microscopy Center.

Author contributions

X.L.W. proposed the concepts of the intrinsic TE performance and fast melt-quenching method for the $Cu_{2-x}Se$ system. X.L.W. and L.L.Z. designed the experiments. L.L.Z. performed all the experiments and measurements. X.L.W. and L.L.Z. analyzed the results and co-wrote the paper. All authors contribute to the discussions of the paper.

Additional information

Supplementary information accompanies this paper at http://www.nature.com/scientificreports

Competing financial interests: The authors declare no competing financial interests.

How to cite this article: Zhao, L.-l. *et al.* Superior intrinsic thermoelectric performance with *zT* of 1.8 in single-crystal and melt-quenched highly dense $Cu_{2-x}Se$ bulks. *Sci. Rep.* 5, 7671; DOI:10.1038/srep07671 (2015).

This work is licensed under a Creative Commons Attribution-NonCommercial-NoDerivs 4.0 International License. The images or other third party material in this article are included in the article's Creative Commons license, unless indicated otherwise in the credit line; if the material is not included under the Creative Commons license, users will need to obtain permission from the license holder in order to reproduce the material. To view a copy of this license, visit http://creativecommons.org/licenses/by-nc-nd/4.0/